Available online at www.sciencedirect.com
ScienceDirect
Journal of Hazardous Materials 140 (2007) 444–464
Journal of Hazardous Materials
www.elsevier.com/locate/jhazmat

Review

LNG fires: A review of experimental results, models and hazard prediction challenges

Phani K. Raj *

Technology& Management Systems, Inc., 102 Drake Road, Burlington, MA 01803, USA

Available online 15 October 2006

Abstract

A number of experimental investigations of LNG fires (of sizes 35 m diameter and smaller) were undertaken, world wide, during the 1970s and 1980s to study their physical and radiative characteristics. This paper reviews the published data from several of these tests including from the largest test to date, the 35 m, Montoir tests.

Also reviewed in this paper is the state of the art in modeling LNG pool and vapor fires, including thermal radiation hazard modeling. The review is limited to considering the integral and semi-empirical models (solid flame and point source); CFD models are not reviewed. Several aspects of modeling LNG fires are reviewed including, the physical characteristics, such as the (visible) fire size and shape, tilt and drag in windy conditions, smoke production, radiant thermal output, etc., and the consideration of experimental data in the models. Comparisons of model results with experimental data are indicated and current deficiencies in modeling are discussed.

The requirements in the US and European regulations related to LNG fire hazard assessment are reviewed, in brief, in the light of model inaccuracies, criteria for hazards to people and structures, and the effects of mitigating circumstances. The paper identifies: (i) critical parameters for which there exist no data, (ii) uncertainties and unknowns in modeling and (iii) deficiencies and gaps in current regulatory recipes for predicting hazards.

Keywords: Pool fire; Vapor fire; Emissive power; Spectral irradiance; Flame speed; LNG pool; Atmospheric absorptivity; Hazard criteria

Contents

* Tel.: +1 781 229 6119.
E-mail address: tmsinc1981@verizon.net.

0304-3894/$ – see front matter © 2006 Elsevier B.V. All rights reserved.
doi:10.1016/j.jhazmat.2006.10.029

1. Introduction

Natural gas, which contains primarily methane (CH_4), has been used as an industrial and residential fuel for heating and other purposes for over a century. The density of natural gas at the normal temperature and pressure (293 K and 1 atmosphere pressure) is 0.667 kg/m^3; hence, it is lighter than air at the same conditions. When natural gas is cooled at ambient pressure to a temperature of about 111 K it liquefies to a liquid of density 425–450 kg/m^3; that is, the gas volume is reduced by a factor of about 640–670. Because of this large reduction in volume from gas to liquid, the economics of transportation and storage of considerable amounts of energy as a liquid have favored the development of the liquefied natural gas industry.

The first LNG gas plant in the US was built in West Virginia in 1912 (ref. [1]), while the first commercial liquefaction plant was built in Cleveland, OH, in 1941. Today there are 113 active LNG facilities spread across the United States, including four on-shore import terminals built between 1971 and 1980 (Lake Charles, LA; Everett, MA; Elba Island, GA; Cove Point, MD) and one off-shore facility (Gulf Gateway Energy Bridge Deep Water Port of Excelerate Energy, TX) which began operation in April 2006. In January 1959, the world's first LNG tanker carried LNG from Lake Charles, LA, to Canvey Island, UK. This voyage demonstrated that large quantities of liquefied natural gas could be transported safely across the ocean. Large importation into the US has been continuing since 1976, although after reaching a peak volume in 1979 the quantity imported declined, rather drastically, due to both deregulation of natural gas in the US and price disputes with Algeria (the then sole provider of LNG to the US). In the period 1979 and 2001, the only operating import terminal in the US was the Everett, MA facility. Due to increased demand in early 2000s not only have the Elba Is. and Cove Pt. terminals been reactivated, but also there are over 40 proposals before the Federal Energy Regulatory Commission for building new import and processing terminals in the US.

LNG, a cryogenic liquid, when spilled on land or water evaporates by boiling due to heat transfer from the substrate (and to lesser extent due heat input from the atmosphere and the sun) producing vapors. The predominantly methane vapor that is released is flammable in volumetric concentrations in air between 5% and 15%. If an ignition occurs immediately during the release of LNG, the liquid pool formed on the substrate can sustain a "pool fire." If ignition of the vapor cloud in the open occurs during the time that the liquid is still evaporating, a flash fire occurs in the vapor cloud, which propagates to the liquid pool and results in a pool fire. Much delayed ignition of the vapor cloud, after all liquid has been evaporated, results in a vapor cloud fire only. Depending upon the density and porosity of any obstructions enveloped or surrounded by the vapor cloud during its dispersion, the flash fire can accelerate to form a fast deflagration fire. The concentration of vapor in the cloud close to the location of such obstructions has significant effect on the magnitude and duration of acceleration of the flames. The hazard to people and objects outside a pool fire or a vapor cloud fire arises primarily from radiant heat emitted by the fire. Depending upon the location of a person relative to the fire, the duration of exposure and certain other parameters (discussed later in this paper) exposed skin of a person may suffer pain, burns or other detrimental effects. It is the magnitude and extent of burn hazards posed by the flammable property of LNG that is of great concern to the public.

There has been only one large industrial accident involving LNG; in 1944 LNG was released from a storage facility in Cleveland, OH due to what has been determined to be the failure of the container material (due to its incompatibility with the cryogenic temperature). Unfortunately, the accident resulted in both direct and indirect fatalities. Since then more stringent regulations and standards have been promulgated mandating the use of cryogenic materials for storage tanks and the design of the facility to contain any spilled LNG. In addition, the operational safety and training of personnel have been significantly improved, and construction and operation of large ships have been undertaken with significantly improved technology. Because of these changes in the codes and the commitment to safety of the companies, worldwide, the industry's safety record since "Cleveland" has been impressive; not a single person of the general public (which does not include facility workers) has been exposed to any type of hazards from LNG anywhere in the world.

Not withstanding the above safeguards there is considerable concern on the part of the public, and to some extent by government regulators, about the potential hazards that LNG poses during its storage and transportation, especially because both the size of shipments and storage capacities in terminals are increasing. While in the 1970s such safety questions were based on accidental releases, in the post 9/11 periods the potential actions of terrorists are weighing heavily on the minds of people. In the 1970s and 1980s, the safety questions resulted in the conduct of numerous field tests to understand the types, characteristics and extent of hazards posed by LNG fires on land and

Nomenclature

C_a	constant pressure specific heat of air (J/kg K)
C_S	mass concentration of smoke particles in the fire (kg smoke/m^3)
D	diameter of the base of the fire (or liquid pool diameter) (m)
D_{eq}	equivalent diameter of a trench fire (m)
·	Damkőhler number = $\{\Delta H_C/C_a T_a\}$
$E(Z)$	emissive power of the fire nominal surface at axial position Z (kW/m^2)
E_B	blackbody emissive power (kW/m^2)
E_0	emissive power of the fire nominal surface near the base (kW/m^2)
E_{eff}	effective surface emissive power in the smoky regions of fire (kW/m^2)
E_{max}	blackbody emissive power at the base flame temperature (kW/m^2)
E_S	emissive power of the fire nominal surface covered by smoke (kW/m^2)
E_λ	spectral irradiance (kW/m^2 μm)
$F_{dA_1 \to A}$	view factor between elemental area dA_1 on the fire and A the object area
F	Froude number = $(\dot{m}''_f/\rho_a\sqrt{gD})$
F_c	combustion Froude number = $F \times$ ·
g	acceleration due to gravity (m/s^2)
ΔH_c	heat of combustion of the fuel (J/kg)
k_m	specific soot extinction area (m^2/kg)
L_b	beam length = 0.63D, for cylindrical fires (m)
L_C	length (height) of the bottom "clean burning zone" (m)
L_F	mean length (height) of the visible fire plume (m)
L_I	length (height) of the intermittency zone (m)
$\dot{m}''_f$	mass flux of fuel vapor at the base of fire= $\rho_L \dot{y}$ (kg/s m^2)
$P_w^{sat}(T_a)$	saturated water vapor pressure at T_a (N/m^2)
$\dot{q}''$	radiative heat flux received by an object at distance S (kW/m^2)
r	air to fuel mass ratio for stoichiometric combustion
RH	atmospheric relative humidity (%)
S	distance from the center of the fire (m)
T_a	dry bulb air temperature (K)
U_{wind}	wind speed (m/s)
U^*	dimensionless wind speed
W	width of the trench fire (m)
Y	fraction of the burning fuel that gets converted to smoke
$\dot{y}$	linear burn rate in units of liquid pool regression (m/s)
κ	overall extinction coefficient of the fire (m^{-1})
ρ_a	density of air (kg/m^3)
ρ_L	density of liquid in the pool that is burning (kg/m^3)
τ	atmospheric transmissivity
τ_s	transmissivity of smoke
τ_λ	transmissivity of the atmosphere for radiation of wavelength λ
χ_R	fraction of combustion energy released that is radiated

on water. Many models were developed to extrapolate the test results for predicting hazards from postulated large spills caused by accidental releases.

The objective of this paper is to review: (i) the data from several of the LNG field fire tests including from the largest test to date, (ii) the state of the art in LNG fire thermal radiation modeling, and the accuracy of prediction, (iii) evaluate the adequacy of current models in their applications to situations that are several orders of magnitude larger than those used in test conditions, and (iv) discuss the adequacy of current regulations for public protection.

The calculation of LNG fire hazards involves consideration of three principal issues. These are: (a) description of the characteristics of the fire, namely, its physical dimensions and radiant heat emission (both in magnitude and distribution over its physical form), (b) the reduction in radiant intensity due to absorption/scattering in the intervening atmosphere and complete absorption and/or reflection by intervening objects and (c) the receptor characteristics for absorbing infrared radiation and response. This paper will discuss the "LNG fire hazards" from the above perspective.

2. Experimental investigations

Over the past 30+ years several LNG fire tests have been conducted both in the US and abroad to understand the fire characteristics and the thermal radiation emission from these fires [2]. Broadly, two types of fire tests have been conducted, namely, fixed size pool fires on land and expanding pool fires on water. Table 1 lists some of the important fire tests of the past 3 decades. Significantly, more tests have been conducted on land-dike fires than with pool fires from LNG spills on water. The fire sizes have ranged from about 2 m to 35 m in diameter on land. In the only one set of pool fire tests on water, the maximum diameter achieved was about 15 m. Other parameters measured in these tests are also indicated in Table 1. Discussed below, in brief, is a summary of the various tests and their results.

2.1. Fire tests on land

2.1.1. Esso tests

May and McQueen [3] conducted the earliest of LNG fire tests. These tests involved the measurement of the thermal radiation from a fire on LNG pools in an irregularly shaped trench into which LNG was continuously fed at a metered rate (to maintain a constant liquid level). The thermal radiation field surrounding an irregularly shaped trench was measured using calibrated thermopiles.

Table 1
Summary of LNG fire experiments

No.	Details of field tests			Type of tests	No. of tests	Fire dimensions	Principal results			Technical reference(s)
	Year	Sponsored by	Conducted in				Liquid regression rate (m/s)	Wide-angle radiometer based, mean emissive power[a] (kW/m^2)	Fraction of combustion energy radiated (%)	
1	1969	Esso	Libya	LNG fire in a land diked area (trench): continuous LNG feed	6	70 m long × 25 m widest × 5 m depth (avg). Eq diam = 18 m	1.6×10^{-4}	92	12–16	May and McQueen [3]
2	1962	US Bureau of Mines	Lake Charles, LA	LNG spill on ground surrounded by a dike	NA		–	–	–	Burgess, and Zabetakis [4]
3	1973	AGA	San Clemente, CA	LNG spill on ground surrounded by a dike	7	Diameter = 1.8 m	1.5×10^{-4}	100	20	AGA [5]
					8	Diameter = 6.1 m	2.2×10^{-4}	160 ± 17	25	Raj and Atallah [6]
4	1974–1976	USCG	China Lake, CA	Unconfined pool on water: continuous spill	5	Maximum Diameter = 13 m	4×10^{-4} to 6×10^{-4}	220 ± 47	12–32 (depending on spill rate)	Raj et al. [7]
5	1976	JGA	Japan	LNG spill on ground surrounded by a dike	3	2 m × 2 m square	NA	58	13	JGA [8]
6	1980	British Gas		LNG spill on ground surrounded by a dike	29	Square and rectangular (2.5:1) dikes. Equivalent diameters 6.9 m to 15.4 m	NA		NA	Moorhouse [9]
7	1980	Shell Research	Thornton Research Ctr.	LNG spill into insulated concrete dike	1	Diameter = 20 m	2.37×10^{-4}	153 ± 16	NA	Mizner and Eyre [10]
			Maplin Sands, England	Unconfined pool on water		Mostly vapor fires resulting from delayed ignition	NA	203 ± 35	NA	Mizner and Eyre [11]
8	1981	Tokyo Gas	Japan	Diked pool on land	8	Square pools of 2.5 m × 2.5 m	NA		NA	Kataoka [12]
9	1987	Gaz de France	Montoir, France	LNG spill into insulated concrete dike	3	35 m diameter shallow dikes	3.11×10^{-4}	165 ± 10	NA	Nedelka, Moorhouse and Tucker [13]

[a] Mean surface emissive power is based on the assumption that the flame shape can be described by a tilted cylinder of length given be Thomas' correlation.

The average measured radiation output from the fires was inferred to be 12% of combustion energy released (this number is increased to 16% if the emission from the part of the fire below the rim of the pit is taken into account). The average steady state liquid regression rate was calculated to be 1.6×10^{-4} m/s. The composition of LNG used was about 72% methane; ethane and propane concentrations amounted to about 23%. Because of the relatively high percentage of higher hydrocarbon concentrations it is reported that this LNG fire was not as luminous as it may have been had the LNG contained higher concentrations of methane.

2.1.2. The US Bureau of Mines

Burgess and Zabetakis [4] report a series of both laboratory scale and field scale tests on land to understand the rate of vaporization of LNG (with and without fire), mixing of LNG vapor with air, thermal radiant output as a fraction of combustion energy, etc. The laboratory tests were performed on 0.38 m (15 in.) diameter trays and the field scale tests involved spilling of LNG in to dikes of 3 m × 3 m (10 ft × 10 ft) and 6 m × 6 m (20 ft × 20 ft). The burning rates obtained from the 0.38 m diameter tests indicated a value of 1.94×10^{-4} m/s (0.083 kg/m^2 s). The radiant output fraction measured in the 3 m and 6 m dike fires varied between 20% and 34%. Burgess and Zabetakis conclude that while LNG burning rate is higher than that of gasoline on a volumetric basis, both LNG and gasoline have the same burning rate when expressed on mass basis. That is, the heat release rates from a gasoline fire and a LNG fire of the same size are about the same, since both gasoline and LNG have the same heat of combustion per unit mass (within about 3.5%). In addition, Burgess and Zabetakis conclude that LNG vapors are not explosive even when the large amount of vapor generated by the initial "flash" due to the rapid boiling of LNG on a warm ground surface is ignited. They conclude from this study that LNG can be stored safely, above ground, in properly designed tanks surrounded by dikes "*in the same manner as gasoline storage*."

2.1.3. The American Gas Association

AGA [5] sponsored a series of tests performed at the TRW test facility in San Clemente, CA. These included several LNG pool-on-land fire tests; two different sizes of dikes were used, namely, 1.8 m and 6.1 m. The geometrical characteristics of the fire were measured photographically and the radiation field surrounding the fires was measured using wide-angle radiometers. In addition, the liquid regression rates were measured using a depth gage and the heat flow from the ground to the cold pool was inferred from the temperature data from thermocouples located at different depths in the ground below the center of the pool.

The data obtained from these series of tests have been published by AGA [5]. Within the limitation of the size of fire tests conducted in this series of experiments it is seen that the burning rate, the flame emissive power and the fraction of combustion energy radiated increase with increasing size of the fire diameter. The time-averaged fire emissive power for the larger fire was calculated to be 150 kW/m^2 (range 143–178 kW/m^2). The average values for the calculated fire characteristic parameters obtained from the test data, for the two dike diameters, are indicated in Table 1. Additional discussion of the test data and the results are provided by Raj and Atallah [6].

It was seen in these tests that the fire plume length (or height in calm winds) was about 2–2.5 times the base diameter and that the fire color changed from initial yellow to orange as the LNG pool was consumed. In fact, towards the end a significant quantity of black soot production was seen in the fire. In addition, significant flame plume tilt was seen for wind speeds above a threshold value.

2.1.4. Shell Research Co.

Mizner and Eyre [10] report a series of tests of LNG, LPG and kerosene fires of 20 m diameter. The tests were conducted on pre-cooled (by liquid nitrogen) insulated concrete, shallow dikes. A single 20 m diameter LNG fire test was conducted at a mean wind speed of 6.15 m/s. The burning of pure methane was recorded for over 240 s (in a fire of about 420 s burn time). Even in the early stages of the fire the flame was found to be sooty (with black smoke) in its upper regions. This sooty region began to expand to lower regions when ethane burning was measured. The burning rate of the liquid was found to be quite steady throughout the burning period at about 0.106 kg/s m^2.

The mean surface emissive power (SEP) estimated from the wide-angle radiometer measurements (with the flame shape being described by a bent over cylinder with length equal to the actual measured distance to which flames were visible) during the steady burning period was 153 kW/m^2. Twenty-one, wide-angle radiometers were located down-wind over a 120° arc and radial distances from the dike center of 2*D*, 3*D*, 4*D* and 5*D*. It was found that the standard deviation in the SEP values inferred from the data of these wide-angle radiometers agreed with in 10%. In addition, in these tests steel plates were located on the ground very close to the fire (1.5*D*–2*D* from the center) whose temperature increase due to incident radiant heat flux was measured. The fire SEP inferred from the steel plate temperature measurements was in the range 131–169 kW/m^2, with the mean almost equal to that calculated from wide-angle radiometers.

2.1.5. Gaz de France

Nedelka et al. [13] have conducted the largest LNG pool fire tests to date. In 1987, a series of three 35 m diameter LNG fire tests was conducted on an insulated concrete dike in the field test facility of Gaz de France (GdF) at the Montoir de Bretagne methane terminal in France. The objective of the test program was to understand the burning characteristics of and quantify the radiant thermal emission from large LNG pool fires, in which the dominant heat for the vaporization of the liquid pool comes from the fire. The test series was instrumented with over 40 wide-angle radiometers, 6 narrow-angle radiometers, 2 spectrometers, gages to measure the liquid depth in the dike for obtaining the liquid evaporation rate during the fire, calorimeters located within the dike and just above the liquid surface to measure the heat flux from the fire to the liquid and gas sampling devices within the dike. More details of the instrumentation and details of measured data are published (Nedelka et al. [13], Malvos and Raj [14]). As was found in the 20 m diameter Shell tests, the burning rate was quite steady and methane preferentially burned for over

Source: Gaz de France, Personal Communication

Plate 1. Photograph of the typical shape and characteristics of the fire in test 1, Montoir tests, during the methane steady state burning period.

one half of the duration of the fire. The mean duration of burning of the fires in the three tests was about 450 s. Also noticed was the copious amount of black smoke produced by the burning of the LNG even during the period when only methane was burning. Plate 1 indicates a photograph of the typical 35 m diameter LNG fire observed in these tests. The significant smoke and the "reddening" of the fire in the lower portions can be clearly seen.

The variation in the SEP from the base of the fire to the top of the visible fire was considerable. Fig. 1 shows the narrow-angle radiometer data, uncorrected for atmospheric absorption, in one of the tests. These data refer to the measurement by a narrow angle radiometer that was located at a distance of 155 m from the edge of the dike. Fig. 2 shows the data from the spectrometer that was located 20 m from the edge of the dike. Other findings from the 35 m diameter LNG fire tests can be summarized as follows:

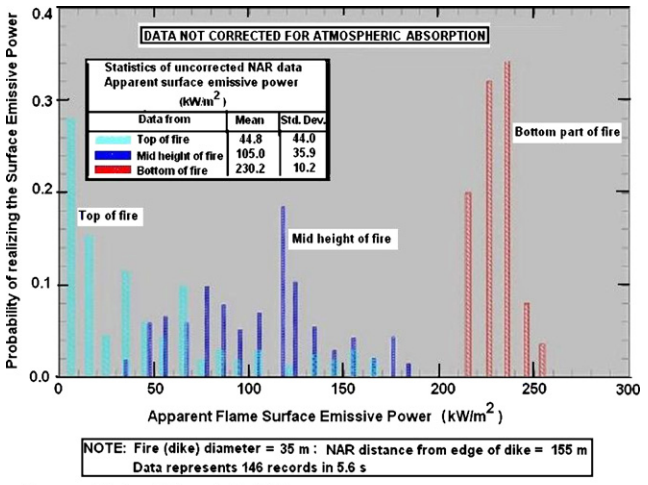

Source of Data: Malvos & Raj [14]

Fig. 1. Statistical distribution of NAR data taken at different times from three locations on the plume of the 35 m LNG fire test # 2.

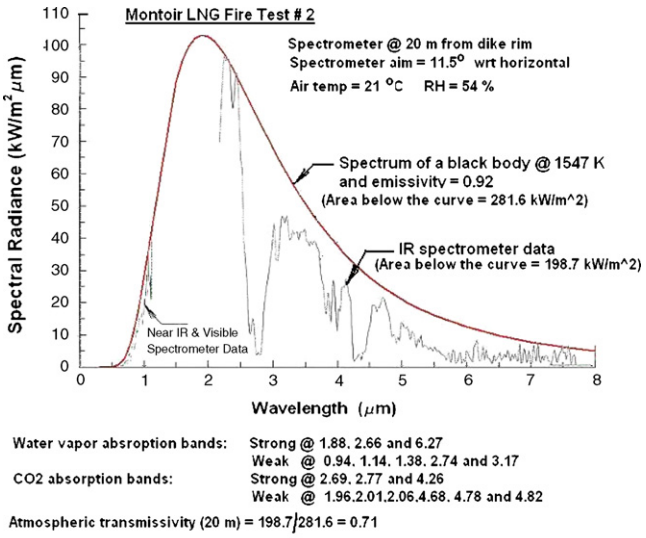

Source of Figure: Malvos & Raj [14]

Fig. 2. Comparison of the data from the IR spectrometer and the visible range spectrometer in the 35 m diameter LNG Fire tests with 1500 K black body spectrum.

(1) The mean liquid evaporation rate due entirely to the heat feed back from the fire is 0.14 kg/m^2 s. This value obtained from the measurement of the actual liquid depth variation with time is considerably lower (by about a factor of 2.5) than the value that can be calculated using the data on the heat flux (from the fire) into the liquid pool measured inside the dike and close to the liquid surface. The discrepancy may be explained as due to: (i) methane vapor absorption of heat radiation at the lower levels of the fire, (ii) absorption and scattering by any liquid droplets thrown up due to the violent boiling inside the pool and (iii) absorption by low temperature soot present close to the liquid surface. Note that the heat input into the pool from the dike floor during the fire test is very small because of the insulated concrete as well as the fact that the floor was pre-cooled.

(2) The 5 s time averaged data recorded by the movable narrow angle radiometer located at 155 m from the dike edge indicate that the apparent spot emissive power (uncorrected for atmospheric absorption) at the bottom of the fires (within a height of 6 m), varies between a low of 79 kW/m^2 to a high of 221.7 kW/m^2. The maximum values recorded in the three experiments are, respectively, 201, 208 and 221.7 kW/m^2. Using the calculated atmospheric transmissivity values (0.65–0.665), consistent with the atmospheric conditions and the location distance to the NAR, the maximum spot emissive power (SEP) ranges from 309 to 333 kW/m^2. Nedelka et al. [13] report that occasionally, the instantaneous SEP (atmospheric absorption corrected) reached 350 W/m^2. It should be noted that because of the "narrow view" of the NARs these SEP values are for a very small region of the fire and do not represent the overall SEPs even in the lower regions of the fire.

(3) The fires in all three tests were very smoky beyond a certain height (or length along the tilted axis). The narrow angle radiometer readings confirm that the time averaged

emissive power of the fire decreases with height (or length along the axis). The mean emissive power calculated from actually visible burning area spots over the entire length of the fire plume was about 265 kW/m^2. The mean emissive power value, based on idealized fire geometry (tilted circular cylinder with axial length given by Thomas' correlation), is reported to be 165 kW/m^2.

(4) The spectral data from the lower parts of the fire indicate that the 35 m LNG fire is not optically thick. It can be characterized by a black body at a temperature of about 1547 K and emissivity 0.92. This emission applies only to those parts of the fire that are luminous. However, considerable smoke at higher regions masks the high emission rate lowering the apparent emissive power averaged over time and fire size.

2.2. Fire tests on water

Very few tests have been conducted with LNG spill fires on water. Also, very limited data are available for the burning characteristics of fire on water as well as thermal radiation values from such fires. Two series of experiments have been reported with the specific objective of measuring the behavior of LNG fire on water. The only series of tests to understand the burning of LNG pools on water was conducted in 1976–1978 in China Lake, CA and reported by Raj et al. [7]. In 1980, Shell Research Ltd., UK conducted tests at Maplin Sands to understand the characteristics of burning of flammable vapor clouds generated by LNG spills on water and dispersed without ignition at the source. In one of these tests, the flashing vapor fire ignited the still boiling pool at the source resulting in a relatively short-lived LNG pool fire (Mizner and Eyre [11]). The details of the above two series of tests and their results, as they pertain to LNG pool fires, are discussed below.

2.2.1. China Lake tests

These tests were conducted spilling LNG at a rapid but controlled rate on to the water surface in the middle of a 50 m × 50 m × 1 m depth pond. The volumes of LNG released ranged from 3 m^3 to 5 m^3. In the "pool fire" tests, an igniter was activated near the spill point as soon as the LNG hit the water surface. This produced an immediate ignition and resulted in an initially expanding, burning pool of LNG with a generally tall and columnar fire plume. An illustration of the resulting fire is shown in Plate 2. The picture shown is that of a fire at about the mid point (35 s) in the duration of burning of the pool (75 s), when pure methane was burning. The fire is tall and yellow in color signifying high radiant emission.

A series of eight pool fire tests was conducted. A majority of tests were conducted under essentially calm conditions so that the fire plume was vertical. In two tests delayed ignition occurred. In three tests, the wind speed was significant. The test conditions and some important results are indicated in Table 2. Fig. 3 shows the narrow-angle radiometer (NAR) data (after correcting for the atmospheric absorption) from this series of tests.

Fig. 4 shows the data obtained from a spectrometer showing the fire emission spectrum. It is seen that the fire is hardly a black body emitter. Clearly, the emission from a fire of these

Table 2
Summary details of China Lake LNG-on-water pool fire tests

Test no.	LNG spill volume (m^3)	Spill duration (s)	Rate of spill = $10^{-2}x$ (m^3/s)	Measured state pool diameter (D) (m)	Duration of intense burning (s)	Burning rate[(1)] = $10^{-4}x$ (m/s)	Measured visible flame length (L) (m)	Mean ratio (L/D)	NAR measured fire emissive power[(2)] (kW/m^2)	Emissive power inferred from WAR data[(3)] (kW/m^2)
1	5.3	254	2.09	8.5	210	4.45	24.0 ± 2.7	2.8	–	–
2[a]	5.3	52	10.19	–	–	–	–	–		
3	4.2	49	8.57	11.5	42	9.63	47.2 ± 3.9	4.1	207 ± 5	–
4	4.2	248	1.69	9.0	195	3.39	25.5 ± 6.3	2.8	200 ± 11	–
5	3.0	32	9.38	12.8	26	8.97	55.0 ± 8.5	4.3	187 ± 29	–
6[b]	5.7	52	10.96	15.0	40	8.06	42.0 ± 6.4	2.8	185 ± 6	–
7[c]	5.7	75	7.60	16.8	75	3.43	–	–	–	–
12	5.7	81	7.04	14.0	75	4.94	44.0 ± 6.3	3.1	224 ± 13	220 ± 47

Notes: (1) The burning rate is calculated as if all spilled LNG burned during the intense burning period over the area given by the mean measured diameter. This gives the upper bound of burning rate. (2) Atmospheric absorption corrected values. In tests 3, 4, 5 and 6 the narrow angle radiometer (NAR) was 60 m from center of fire. In test 12, NAR was 30 m from fire center. (3) Assuming a solid flame of height equal to 3.1 times mean diameter and measured WAR data corrected for atmospheric absorption. WAR data from other tests have not been analyzed. (±) The number after this symbol is to be interpreted as the standard deviation in the value.

[a] Initial high wind blew vapor away from the igniter and resulted in delayed ignition. Hence, there was only a partial pool fire. The data obtained are not representative of pool fire and not analyzed. Entire pool burned in very short time (compared to spill time).

[b] Wind speed was 3.1 m/s. Significant differences were observed in pool dimensions from two different directions. Diameter indicated is the mean of the wind-ward and cross wind dimensions.

[c] This is a delayed ignition pool fire.

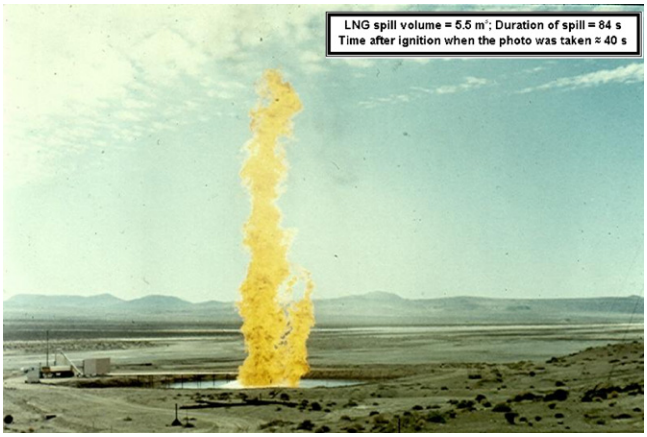

Plate 2. Fourteen metre diameter LNG fire on water in test # 5 of China Lake tests.

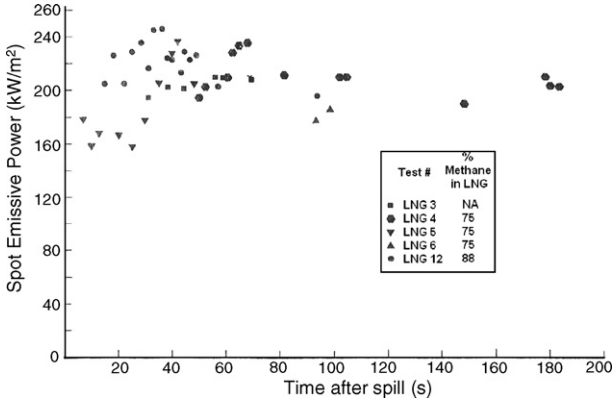

Fig. 3. Narrow angle data on surface emissive power vs. time for China Lake LNG fires on water.

diameters consists of band emissions from water vapor and CO_2 and a continuous emission due to luminous soot. For the China Lake fire (13 m diameter), the emissivities of the luminous soot, water vapor and CO_2 are found to be, respectively, 0.14, 0.19 and 0.35. Also, the flame temperature for the China Lake fire (13 m diameter) is calculated from the spectral data to be close to 1500 K. Detailed analysis of the spectral data has been published recently by Raj [15].

The principal findings from China Lake series of pool fire tests on water are:

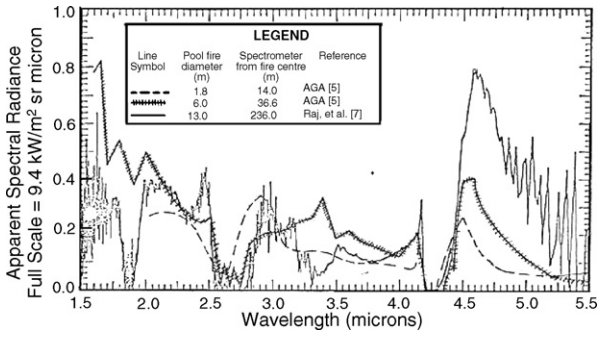

Fig. 4. Typical LNG pool fire spectra from AGA tests and in China Lake test # 5 at 20 s.

(1) The apparent burning rate increases with increase in spill rate. This phenomenon is attributed to the deeper penetration of the spilled LNG into water, its break up and vaporization over a large number of LNG droplet surface area that is considerably larger than is presented by the horizontal (water–LNG) contact area defined by the mean pool diameter.

The burn rate vs. the spill rate is correlated by a dimensional, linear least square fit equation:

$$\text{apparent burn rate } \dot{y}(\text{m/s}) = 10^{-4} \times [2.73 + 58 \times \text{spill rate}\,(\text{m}^3/\text{s})] \quad (1)$$

The above correlation contains the heat flux contributions from water and fire. It is likely that the heat flux from fire-to-pool in fires of diameters larger than the ones in these tests will be different. Hence, it is uncertain whether the above correlation will be applicable to the burn rates of LNG on water with very large pool fires.

(2) The time averaged height to diameter ratio of the visible flame is slightly less than that predicted by Thomas's correlation in the range of the measured burn rates. The height to diameter ratio data is correlated by the following least square linear fit equation on the log–log plot.

$$\frac{L_F}{D} = 46.5\left\{\frac{\rho_L}{\rho_a}\frac{\dot{y}}{\sqrt{gD}}\right\}^{2/3} \quad (2)$$

(3) The energy emitted by the fire as radiant heat, expressed as a fraction of combustion energy generated by burning, decreases with increase in spill rate. Fig. 7 shows the variation of the fraction of combustion energy released as radiant heat (assuming that all evaporated LNG burns in air) versus spill rate. Assuming that the height of the flame is that given by correlation in Eq. (2), it can be shown that the combustion energy fraction varies as $\{\dot{y}\}^{-1/3}$ for a constant diameter and constant emissive power. However, the actual data in Fig. 7 indicates a steeper drop in the fraction radiated compared to the above-predicted rate for spill rates greater than 5×10^{-2} m^3/s. This implies that in high rates of release a part of the released vapor does not burn at all; that is, the faster the vapors are generated, the less the chance for combustion. In much smaller scale tests (0.38 m diameter) involving the spill of LNG on to a warm tray, Burgess and Zabetakis [4] also found that about 70% of the vapor generated initially did not participate in combustion.

(4) The flame emissive power values obtained from the narrow angle radiometer (NAR) and that inferred from wide angle radiometer (WAR) data by assuming a cylindrical shape for the fire and the measured mean height of the fire, agree very closely in their mean values. The mean emissive power of the 14 m diameter fire is found to be 220 ± 47 kW/m^2. However, if the NAR data from all tests are considered (see Fig. 3), the mean and standard deviation of the NAR data are represented by 205 ± 20 kW/m^2. The scatter in the WAR data is about twice the scatter in the NAR data. The large

variation in the computed emissive power from the WAR data is due to the fact that in reality the fire is not a cylindrical columnar fire of constant height but tends to pulsate both in diameter (as the large turbulent eddies rise up through the fire) and in height, whereas the emissive power calculating procedure uses only a constant height and diameter fire. Had the exact shape of the fire at every instant been used to calculate the mean emissive power, the data scatter would have been much less.

2.2.2. Maplin Sands tests

The details of this test series are discussed in the section on "Vapor Fires." In one test (test # 39) of the seven tests with LNG spill onto water in an ocean environment the vapor fire flashed back to the source, which was still in the form of a boiling pool of LNG. This resulted in a LNG pool fire of very short duration (several seconds). The data set from this single, very short-duration *pool fire*, indicates that the visible flame height was in the 40–60 m range (no data are available for the diameter of the burning pool of liquid) and the calculated surface emissive power (based on measurements of the fire size and radiometer data at measured at different times within the short life time of the fire) ranges from 179 to 248 kW/m^2 with a mean value of 203 kW/m^2. This result on SEP compares favorably with those obtained in the China Lake experiments.

2.3. Fires on elongated LNG pools on land

Very limited experimental investigations have been performed on the thermal radiation from trench fires. Trenches form the impoundment areas for collecting any leaks from process equipment, vaporizers and transfer piping in a LNG terminal. Laboratory scale trench fire tests have been reported by Gollahalli and Sullivan [16]. Croce et al. [17] report a series of 13 field scale fire tests with trench sizes varying from 0.82 m (W) × 4.4 m (L) to 3.9 m (W) × 52.1 m (L), covering a range of length to width (aspect) ratios from a minimum of 4.97 to a maximum of 30. The wind speeds during the different tests varied, from a minimum of about 1 m/s to a high of 8.36 m/s. The principal findings from trench fire tests are summarized as follows:

(1) In the laboratory tests, the flame sheet was not coherent for length to width aspect ratios greater than 4. For larger aspect ratios, the flame sheet broke up into distinct columns of flame ("flamelets") with the overall heights of the fire being lower compared to the case of coherent flame sheet.
(2) The heat flux data on the perpendicular bisector to the trench length show an inverse square relationship with the dimensionless ratio of distance from fire center to the equivalent diameter based on the trench area (S/D_{eq}), in both the laboratory and field tests for values of $S/W > 2$.
(3) The flame height to trench width ratio, in the laboratory tests, reaches a constant value after the flame sheet loses coherency. In the tests by Croce et al., the flame height to width ratio decreases linearly with wind speed based Froude number ($Fr' = U_W/2\sqrt{gW}$) up to $Fr' = 0.25$ and then becomes essentially a constant at about 2.5 and independent of Fr'. This implies that at lower wind speeds, increase in wind speed resulted in a decrease in the burning fire plume length; above a critical wind speed flame length is independent of the wind speed.
(4) The fire induced burning rate is much smaller than the fire induced burning rate in a circular pool of equivalent diameter. The steady state burning rate measured in the field tests ranged from 4.3×10^{-2} to 8.0×10^{-2} kg/m^2 s. The burning rate does not seem to correlate with wind speed implying that the bending of the fire has limited effect on the heat feed back to the liquid.
(5) Considerable ground overshoot of the flame in the downwind direction ("flame drag") was noticed in the field tests. The flame drag ratio (1 + downwind extension from the trench edge/trench width) ranged from 1.21 under low wind speeds to 4.23 in high wind speeds.
(6) The flame plume is tilted by the wind—the higher the wind speed the more the tilt from the vertical.
(7) Fire (mean) surface emissive power (SEP) values calculated using the radiometer data from the field tests, the mean measured flame lengths and tilts range from 50 to 200 kW/m^2, the latter from wider trenches. Croce et al., conclude that based on these results it can be postulated that a LNG fire on 6 m width trench would exhibit a SEP of 220 kW/m^2.
(8) The thermal radiation hazard distances can be predicted by using the standard models by considering the fire geometry as rectangular, optical length (in width direction) as 4 m and the maximum SEP of 220 kW/m^2 and using the flame tilt correlations available in the literature by using the trench width as the characteristic dimension of the fire.

2.3.1. Summary Pool Fire test results

In Table 1, the details of the various pool fire tests are presented and also the principal findings from these tests. Fig. 5 shows the results for the mean surface emissive power calculated from the data from different LNG pool fire tests, plotted as a function of the base size of the fire. It should be noted that the SEPs on the *Y*-axis represent the "fire mean" based on the description of the fire plume length (or height) given by Thomas' correlation (see Eq. (6) below). Also plotted in the same figure is the mean SEP for the 35 m diameter Montoir tests, where the SEP is based only on the actual emitting surfaces of the fire

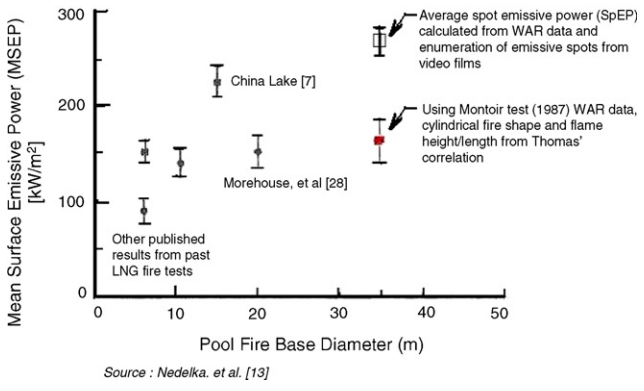

Fig. 5. Calculated emissive powers from different size LNG pool fires.

(rather than the entire geometry of the fire). As can be seen, this number is larger (~275 kW/m^2) compared to the overall, fire size average value (of 165 kW/m^2). The fire size averaged SEP seems to increase with diameter up to about 15 m diameter and then decreases. It is possible to postulate, based on the results in Fig. 5, that a LNG pool fire of diameter 20 m and larger begins to produce significant black smoke (which shrouds the fire) resulting in the diminution of radiant heat emission. The value of SEP for the 20 m fire seems to be lower than for the 35 m diameter fire because the fire may be producing black soot and yet may not be optically thick. However, the 35 m diameter fire, as is seen in Fig. 2, is almost a blackbody emitter and also can be considered to be, more or less, "optically thick."

In Fig. 6 is plotted the ratio of "mean" visible flame plume length (L) and fire pool diameter (D) as a function of the combustion Froude number (see definition in Eq. (7) below) for all pool fire experiments to date. It is seen that the data span a combustion Froude number range of 6×10^{-3} to 2.5×10^{-2}. The L/D ratios vary from about 1.2 to about 3. More discussion on this finding and the extrapolation to other larger size pool diameters is provided in a later section.

2.4. Vapor fire experiments

In the late 1960s and early 1970s Gaz de France [18], TRW [19] and the AGA [20] conducted field tests to study the extent of flammable zone produced by spills of LNG on land. In these tests, the vapor cloud was ignited by one or more torches located at ground level and at different distances on the downwind side of the dike into which LNG was poured. While no direct measurements of either the temperature inside the burning cloud or the radiant heat emission from the propagating fire were made, enough data could be extracted from the video films of the tests to describe the physical characteristics of the vapor fires. Raj and Emmons [21] have performed these analyses by reviewing the video films and other results from these tests and have developed a model for the burning of a vapor cloud in the form of a deflagration fire in the absence of obstructions. It is well known that due to flame wrinkling by obstructions the flame speed increases.

Only two series of tests are reported in the literature with the specific objective of understanding the phenomenon of flame propagation in flammable vapor clouds in the open, ignited by normal ignition sources. In these tests, measurements of the flame propagation velocity, pressure increase in the atmosphere at selected distances outside the flame path, radiant heat emission from the traveling vapor fires, the effect of the igniter location inside the cloud relative to its down-wind edge, etc., have been made. The two test series and their results are discussed in the following sections.

2.4.1. Maplin Sands Vapor Fire tests

Mizner and Eyre [11] report a series of tests performed by Shell Research Ltd., UK in1980 involving the spill of LNG (and LPG) on to the sea and ignition of the vapor cloud formed. A total of seven LNG spill tests and four LPG tests were conducted. The objective of the tests was to understand the thermal radiation from a vapor cloud fire formed by the ignition of a cloud generated by spill of a cryogenic flammable liquid on to water and the dispersion of the cloud on water. All LNG tests resulted in the ignition and complete combustion of the spilled LNG after it had been dispersed in the form of a vapor cloud. The vapor fire in all cases flashed back to the source in the form of a deflagration fire. Radiometers were provided (on a number of pontoons stationed on water over several concentric semi circles with the spill point as the center) to measure the radiant heat flux from vapor cloud fires. The farthest semi circle containing the radiometers was of radius 650 m.

The measured flame heights of the vapor fires were in the 10–20 m range and the flame height-to-width ratios during he cloud fires stages were in the 0.2–0.5 with wide scatter. The mean surface emissive power (SEP) of the *vapor fires* ranged

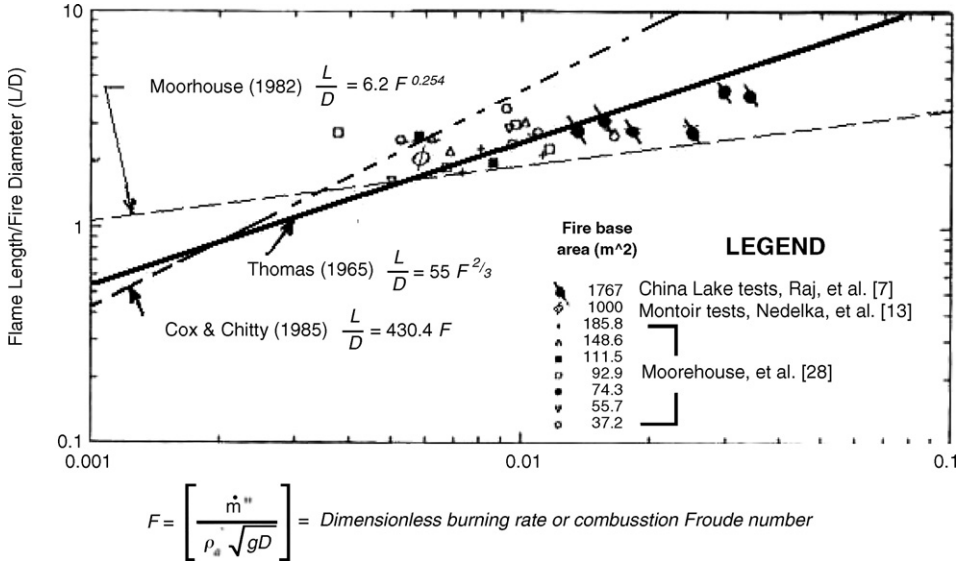

Fig. 6. Comparison of experimental data on fire height-to-diameter ratios with correlations for use in models.

between 138 and 226 kW/m^2 with standard deviations in the 7–15% range. It should be noted that in these test series the fire was well ventilated and the vapors were well mixed with air; therefore, the fires behaved more like pre-mixed flames than diffusion fires.

2.4.2. Coyote series of tests

Rodean et al. [22] report the results of a series of five LNG vapor cloud fire tests ("Coyote" series) conducted in 1981 by the Lawrence Livermore National Laboratory (LLNL) to determine the characteristics of fires resulting from the ignition of dispersed vapor clouds resulting from LNG spills. A further objective of these series of tests was to determine if non-energetic ignition of the vapor cloud would result in explosive burning of the vapor cloud. The tests involved the spill of LNG on to the water surface in the middle of a pond 58 m in diameter and igniting the vapor cloud formed at a selected downwind location on land. Three tests with LNG (of methane concentrations varying from 75% to 81.5%) and one test with liquid methane (LCH_4) are reported. The spill quantities varied from 14.6 to 28.6 m^3 (LNG) and 26 m^3 (LCH_4) and the spill rates from 13.5 to 17.1 m^3/min. Mean wind speeds varied between 4.6 and 9.7 m/s over the series and wind speeds were variable both in speed and direction within the duration of a test. This series of test forms a set of well instrumented vapor fire tests; instruments measured such items as the heat flux to objects within the "burn zone," radiant heat flux at several locations outside the vapor fire zone, flame velocity, ground heat input to the cloud, vapor concentrations in the cloud, etc. In addition, there was extensive photographic data taken with both IR and visible video instruments both from the sides and from the top ("bird's eye view").

The ignition of the vapor cloud was initiated only after the cloud had been fully established so that the LFL distance downwind was a maximum, as measured by the concentration sensors. Pre-ignition maximum down wind distance to LFL varied between 145 and 218 m. Igniters were located downwind of the spill point on land at 61, 79, 79 and 85 m, in the respective tests; hence, ignition was not from the front edge of the cloud but from within it and at approximately half the distance on the centerline to the down wind LFL extent.

Important findings from the Coyote series related to the ignition within the center of the cloud are:

(1) The fires on the lower concentration cloud burning regions were very blue in color.
(2) The cloud burning phenomenon and the production of hot gases there-from result in the "pushing" and the consequent expansion of the pre-ignition 5% (LFL) contour area. The maximum downwind burn distances were 85–90% of the dispersion-based estimates.
(3) Burn areas were not in the same location as the pre-burn 5% contour areas but considerable meander was noticed. Propagating flames did not go beyond the 5% gas concentration locations.
(4) The relationship of the total burn area to the pre-ignition 5% contour area is not clear from the data. In one test, the burn area was smaller than in the 5% contour area whereas in another test it was about 150% of pre-ignition, 2 m level flammable area. However, in the one test there was a rapid phase transition (RPT) explosion. In addition, there was significant instantaneous generation of gas, which then moved downwind as a unit. The burn area in this test was almost two times the measured pre-ignition flammable area.
(5) Flames were hardly visible in the lean concentration parts of the cloud whereas the burning vapor cloud, upwind and closer to the vapor source had a yellow (and visible plume) flame. This is attributed to higher concentration (and higher hydrocarbon content) of vapor in the cloud. Ratio of visible flame height to pre-ignition visible cloud height was in the 5–10 range.
(6) By and large the flame speeds measured with respect to the ground had similar magnitudes both in the downwind and upwind direction. The initial velocities, immediately in the vicinity of the igniter were greater than at farther distances. Upwind flame propagation velocities were slightly higher than those of downwind propagation. However, the turbulent flame speed relative to unburnt gas does not seem to correlate well with wind speed.
(7) No flame acceleration was noticed; on the contrary, all fires seem to have higher flame velocities (relative to the ground) near the ignition sources. The flame speeds with respect to ground were close to 30 m/s near weak ignition source tests and about 40–50 m/s in the jet ignition test. However, the flame speeds rapidly decreased to essentially constant speeds of 10–15 m/s within about 50 m.
(8) Pressure increase measured in the atmosphere due to the propagation of fire was in millibars and hence inconsequential.
(9) The heat fluxes measured inside the fire were in the 150–340 kW/m^2 range. The surface emissive power of the yellow flame (seen when the cloud near the vapor source was burning) is calculated to be in the 220–280 kW/m^2 range.

2.4.2.1. Summary Vapor Fire test findings. The principal findings from the field experiments reported in the literature on dispersed LNG cloud vapor fires in the open can be summarized as follows:

(1) When the vapor cloud is ignited at downwind locations, a turbulent fire propagated to the vapor source (against the wind).
(2) The velocity with respect to the unburnt gases ("flame speed") of the flame front moving into the unburnt vapor was at a more or less constant velocity in a given test. The data from a number of different test series are plotted in Fig. 8. Based on the results presented in this figure, it is seen that the flame speed increases, more or less linearly with the wind speed according to the formula $U_F = 0.8 + 1.6 \times U_W$. It is noted that the laminar burning velocity of the stoichiometric concentration of methane in air is 0.4 m/s. Because of natural turbulence in the atmosphere, even at zero wind speed, it can be argued that the burning velocity of stoichiometric mixture of methane and air will be higher than the

laminar burning velocity. This is clearly seen in the least square fit equation above. It should also be noted that the above correlation represents a mean burning velocity over all concentrations in the vapor cloud (and not just the stoichiometric concentration), especially, the higher than upper flammability limit (UFL) concentrations.

(3) When ignition occurs within the cloud the flame speeds with respect to the ground seem to be constant in both upwind and downwind directions; however, the correlation of the flame speed with respect to the unburnt gas is very poor.

(4) A burning zone supporting a fire plume follows the flame front. The height of the fire plume is dependent on the concentration of the unburnt gas. The higher the concentration, the greater is the fire plume height (diffusion fire). In regions of vapor cloud where the concentrations were in the LFL to UFL the flame height was essentially equal to the vertical depth of the cloud and the flame was hardly visible. Also, the width of the burning zone (in the direction of propagation of the fire) was dependent on the longitudinal concentration gradient (prior to the flame propagation).

(5) Objects or even undulations in the ground, which acted as flame holders, could arrest the flash back of the fire to the source. This phenomenon has not been fully investigated but seems to indicate that flame holder effect would occur only in high concentration parts of the cloud. Plate 3 shows such a "flame holder" phenomenon at the edge of the pond.

(6) The ratio of the height of flames to the initial depth of the (visible) cloud is between 5 and 10 for in-cloud ignition. Also, in this type of ignition, the burnt gases produced within the middle of the cloud push the rest of the unburnt gas, thereby expanding the 5% concentration contour with time (over and above that caused by atmospheric turbulent dispersion). It should, however, be noted that the height of the fire plume is dependent on the mean concentration of the cloud at the location of the fire rather than on the depth of the visible layer, which depends very strongly on the atmospheric relative humidity and mean vapor concentration.

(7) The area of burn seems to vary with the type of ignition and the concentration of the gas at ignition point. In some cases, the total burn area could be as high as 200% of the pre-ignition area within the 5% (LFL) contour. This difference, noticed in the Coyote tests, has been attributed to the hydrodynamics of expansion of burnt gases pushing the unburnt gas in a center-of-cloud ignition and the effects of RPT's in some tests that resulted in a series of puffs of gas traveling down-wind at the time of ignition.

(8) The thermal radiation from the burning cloud to objects outside the fire can be evaluated by assuming the fire to have a SEP of 220–280 kW/m^2. The extent of radiant thermal hazard distance from the edge of the cloud will depend upon both the mean SEP of the fire and the height of the visible fire plume, which itself is dependent upon the local vapor concentration and the wind speed.

(9) None of the vapor tests conducted with a weak ignition source or a jet flare ignition in the open have lead to flame acceleration or explosive ("detonation") burning of a LNG vapor cloud, not withstanding the presence of high concentrations of higher hydrocarbons (ethane and propane) in the LNG. No pressure increase in the atmosphere was measured above a few millibars.

Plate 3. Vapor cloud fire in China Lake test. Fire held at pond' edge during flashback due the flame holder effect from the elevation difference between ground and water levels.

2.5. Fire ball type of burning of LNG vapors

There have been some concerns in the literature on the potential burning of a LNG vapor cloud in the form of a fireball leading to significant radiant heat release and, hence, higher hazard distances. Until recently, there were no controlled tests to understand this phenomenon or the conditions under which such fireball type of burning could occur. Also, the characteristics of the fireball had not been investigated. Tests conducted in 2000 by Gaz de France and reported by Daish et al. [23] provide the first experimental data on such fires.

2.5.1. Gaz de France Experiments

A series of controlled vapor fire tests was conducted to understand the burning of vapor clouds of LNG in the open and to determine the phenomenon of fireball type burning. Medium-scale tests were carried out with LNG vapor clouds being produced with controlled emission of LNG vapor with high gas concentrations in order to study fireball formation. High-concentration vapor clouds with low momentum were generated by spilling LNG into a pit (1.8 m diameter and 1.7 m deep) consisting of pebbles to simulate a very large LNG spill due to an accident and significant vapor generation. Ten experiments were performed in total. In each test, the objective was to generate a cloud with a substantial volume above the UFL and then to ignite the cloud at various locations relative to the flammable volume to determine the effect of placement of igniter relative to the high concentration parts of the cloud. Radiometers, gas concentration sensors, igniters, thermocouples were placed at several radial positions at the intersections of 10° sectors with the radial lines. Video and photographic records were also made of the tests. Seven tests were conducted with electric spark igniters and the others with flares. In the seven spark ignition tests, the igniters that were fired were located at 10.8 m (radially from the center of spill) except in one test where it was at 20.9 m. Fuel release rates ranged from 2.6 to 5.6 kg/s. The estimated UFL and

LFL radial distances were 5–7.5 m and 15–30 m, respectively. That is, the ignition was within the cloud concentrations of LFL and UFL. The mass of LNG vapor within the LFL zone was estimated to be in the range 8.2–19.2 kg.

The fire produced varied between the trials. The fire was characterized by high and wide flames, propagating over the entire cloud area and generating fireballs, or the fire was observed to be traveling from the middle to the borders of the cloud without the generation of a fireball. The most significant finding from these tests was that some form of identifiable fireball event was observed in at least 6 of the 10 trials. It appeared that ignition of a cloud with a large vapor-rich volume led to strong combustion and heat generation over a sufficiently localized area that a self-sustaining motion entraining fuel and air was generated and continued until most of the fuel was exhausted. This burning mode had a distinctive "starting thermal" type of characteristic that distinguished it from other burning modes. The diameter of the observed fireballs ranged from 5 to 30 m and the height to which the fireballs rose ranged from 17 to 26 m. Measurements at 20 m distance indicated a very rapidly varying heat flux with a duration corresponding to the lifetime of the fireball and reaching, in one test, as high as 50 kW/m^2 lasting only for a few seconds. The temperatures measured within the fire ranged from 928 to 1243 K. No surface emissive power data or the rise time of the fireballs has been provided in the data sets.

While there are no other controlled tests to determine the conditions under which fireballs occur from the ignition of LNG vapor clouds, it is reported Brown et al. [24] that a fireball type of fire was observed due to an accidental ignition of a high concentration LNG vapor cloud in Falcon series of tests (conducted by Lawrence Livermore National Laboratories, LLNL). In Falcon test # 5 a RPT occurred and high concentration cloud of vapor formed was ignited by an unknown ignition source (speculated to be a piece of pipe insulation saturated with oxygen condensed from the air). No quantitative data on this fireball are available.

In summary, it is not certain from the data gathered in the Gaz de France experiments what the exact criteria are under which an already dispersed cloud would exhibit a fireball type burning behavior. The qualitative conclusion seems to be that if a LNG vapor cloud is ignited at a location between the LFL and UFL concentrations, and a substantial mass of the cloud is still in regions above UFL concentration, then a fireball type burning is possible. No mathematical criteria have been developed relating the physical size of the cloud, the mass of vapor above UFL and the type of igniter that will lead to a fireball type burning. It is also not clear from the data whether the fireball type burning would result in a larger total thermal burn hazard area compared to that from a spread out cloud which when ignited results in a flash fire (and burns almost everything within the fire area) and poses radiant heat hazard to near field distances from the edge of the burn zone. A rising fireball only poses the hazard due to the transient thermal radiation field and not much by its physical size (compared to a spread out cloud). Therefore, the question of the comparative extent of potential hazards from any fireball type of burning from a LNG vapor cloud is at present not completely answered.

3. Fire hazard prediction models

In many forums, the public has expressed considerable concerns on the safety in LNG transportation, handling and storage. The principal concerns are related to the dangers posed to both people and objects by large LNG spills followed by pool fires, vapor fires or explosions. In the case of pool fires (either on land or on water), the distance to which the radiant thermal hazard extends is the parameter of concern, while in the case of vapor fire the total area occupied by the vapor cloud (prior to burning) and the extent of radiant thermal hazard zone surrounding the initial flammable vapor cloud foot print are the parameters of concern. The postulated sizes of spills and the dimensions of the pools and sizes of vapor clouds are large; for example, in a recent report, the Sandia National Laboratory (Hightower et al. [25]) predict, for spills from a LNG ship, liquid pool sizes on water of over 500 m diameter (for largest spills), sustaining a pool fire. Similarly, a non-ignited LNG vapor cloud generated by the same type of spills dispersed in the atmosphere extends 2.4–3.6 km from the source. Obviously, the scales of these phenomena are larger by orders of magnitude than any test that has been conducted (or will be conducted). Hence, to assess the potential hazard consequences of such postulated releases sound physical models validated against available test data and extrapolated with proper physics are essential. Discussed below is the state of the art in modeling pool fire and vapor fire phenomena.

3.1. LNG pool fire models

The radiant heat flux to an object outside a pool fire depends on: (i) the size, shape (geometry) and the radiant emission characteristics of the fire, (ii) the transmissivity of the atmosphere intervening between the fire and the object, (iii) the location and orientation of the object relative to the fire and (iv) the object properties, such as the spectral reflectivity and absorptivity. Whether the object suffers damage or not depends, in addition, on its thermal properties (duration of exposure to the radiant heat, external cooling, thermal inertia and the temperature at which damager occurs). Two general, semi-empirical approaches (excluding CFD modeling), are described in the literature to calculate the heat flux to an object from a pool fire. These are discussed below.

3.1.1. Point source model

This model is based on the inverse square law of radiation. The heat flux incident on an object at a distance S from the center of a fire of diameter D is calculated using the following equation

$$\dot{q}'' = \chi_R \frac{\left[(\pi/4)D^2 \dot{m}''_f \Delta H_C\right]}{4\pi S^2} \quad (3)$$

Implicitly assumed in the above representation are the assumptions that: (i) all of the radiant energy is liberated at a point on the ground, (ii) the intervening atmosphere does not absorb any thermal energy and (iii) the object is a small vertical surface element on the ground.

Based on radiant heat flux measurements discussed in Section 2.2, the value of the fraction of combustion energy radiated

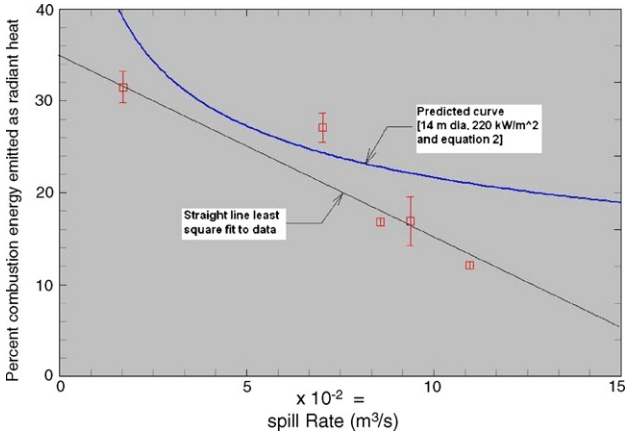

Fig. 7. Fraction of combustion energy radiated as a function of the spill rate in China Lake tests and comparison with theoretical estimates.

(χ_R) is shown to vary between 12% and 32% (see Fig. 7 and Table 1). It is anticipated that for larger diameter fires the fraction radiated will decrease due to smoke obscuration effects, and simple geometry effects (i.e., the heat generation rate is proportional to fire base area whereas the emitting surface area increases, approximately, as $D^{1.7}$). Data presented by McGrattan et al. [26] *for heavier hydrocarbon fuels* (other than LNG), shows the following correlation for the fraction radiated with fire diameter,

$$\chi_R = 0.35e^{-(D/20)}; D = \text{fire diameter in meters} \quad (4)$$

This correlation, if applied to a 15 m diameter LNG fire, predicts $\chi_R = 0.17$, a value tantalizingly close to a measured value (in the China Lake experiments) of 0.125. However, this can only be considered as a coincidence; the application of the above correlation to the Montoir 35 m diameter fire yields $\chi_R = 0.06$ and application to a 100 m diameter fire results in $\chi_R = 2.36 \times 10^{-3}$. Of course, such predictions are not only unsubstantiated but also seem to be ridiculously low for large fires.

This model has considerable difficulty in its application to any serious assessment of potential hazards, because of its rather simplistic representation of both the fire and the receiving object, and the fact that the fraction of energy radiated is not an intrinsic property of combustion and depends upon a number of factors including the rate of spill (as shown in Fig. 7).

3.1.2. The solid flame model

This model is based on semi empirical correlations and represents a fire as a surface emitter of radiant heat energy. The model represents the fire by a geometrical shape (and its orientation due to wind effects), assigns either uniform or variable surface irradiance (also termed "Surface Emissive Power", SEP), and includes the transmissivity of radiant heat in the atmosphere, the relative distance and orientation of the radiant heat-receiving object. The mathematical representation of the model is given by:

$$\dot{q}'' = \sum_{i=1}^{N} F_{dA_i \to A_{obj}} \int_{\lambda} (E_{\lambda,i}\, d\lambda)\tau_{\lambda,dA_i} \quad (5)$$

where $\dot{q}''$ is the radiative heat flux received by an object located at a specified distance from and orientated in a specified angle to the fire, $E_{\lambda,i}$ is the wavelength dependent spectral radiance at an elemental surface on the fire (ith "node"), $F_{dA_i \to A_{obj}}$ is the contribution to the overall geometric view factor from the elemental area on the fire (at position "i") calculated by methods published in the literature, example, by Hottel and Sarofim [27], τ_λ is the wavelength dependent spectral transmissivity of the atmosphere between the elemental surface on the fire and the object, λ is the wavelength of the radiation. Simplified versions of the above model are used in most circumstances (including for regulatory purposes) by assuming a constant (and wavelength independent) emissive power over the entire visible surface of the fire, atmospheric transmissivity independent of the wavelength and assuming the fire shape to be that of a cylinder of base diameter equal to that of the burning liquid pool. The descriptions of the simplified model are described in previous publications (Raj [2,6], Moorhouse and Prichard [28], Considine [29], SFPE [30]).

3.1.2.1. Fire characteristics.

3.1.2.1.1. Fire shape. In most "solid flame" models the shape of the fire is chosen to be a circular cylinder of diameter equal to the base diameter of the fire and axial length representing the visible plume of the fire. The axis of this cylinder is assumed to be vertical in low wind speeds and to tilt with the tilt angle dependent on the wind speed, above a critical wind speed that is dependent on the diameter and liquid evaporation rate ($U^* > 1$, see Eq. (8) below). Moorehouse [31] has proposed a correlation for the overshoot at ground level of the fire extent (due to wind drag). In some models an elliptical shape is used for the horizontal cross section of the cylinder representing the fire. However, it is cautioned that when an emissive power value from the literature is used in a model, the shape of the fire used in reducing experimental data (to obtain a fire-mean emissive power) must be used; otherwise significant errors can result in estimating the radiant heat flux field around the fire.

3.1.2.1.2. Fire plume length (L). Correlations of the following type due originally to Thomas [33,34] have been used in the models to calculate the fire plume length for a fire of diameter D.

$$\frac{L_F}{D} = AF^p(U^*)^q \quad (6)$$

where A, p and q are correlation constants,

$$F = \frac{\dot{m}''}{\rho_a\sqrt{gD}} = \text{Froude number} \quad (7)$$

and

$$U^* = \frac{U_{wind}}{[(\dot{m}''/\rho_a)gD]^{1/3}} = \text{dimensionless wind speed} \quad (8)$$

Many models, such as LNG FIRE 3 by GRI [32], use Eq. (6) with $A = 42$, $p = 0.61$ and $q = 0$ for estimating the visible height of the flame; that is, no wind effects on the visible plume length are assumed. Thomas [33] modified his previous correlations (with no wind condition) to take the wind effect on length by

using $A = 55$, $p = 2/3$ and $q = -0.21$ in the correlation indicated in Eq. (6).

Using a single value for the exponent on the Froude number (F), over the range of F values encountered in fires, to determine the fire plume length is incorrect. Thomas [34] has provided data that indicate different values for the exponent (p) in different value ranges of F; $p = 0.4$ for $F > 10^{-1}$; $p = 0.61$ for $10^{-2} < F < 10^{-1}$ and $p = 2/3$ for $F < 10^{-2}$. In fact, it can be shown from a simple analysis of air entrainment (Raj [35]) that $p = 2/3$, if the fire length (L) is defined as the location by which the fuel is completely consumed within the plume by burning. The same $p = 2/3$ correlation has also been indicated in a book by Murgai [36] based on analysis of forest fire data. Moorhouse [31] has proposed a correlation with $p = 0.254$. Heskestad [37] shows data for a large span of F ($10^{-3} < F < 10^{0}$) indicating varying values for the exponent (p). Cox and Chitty [38] report laboratory experiments in which the visible flame heights of natural gas flames in square burners of sizes 0.3 m × 0.3 m, 0.45 m × 0.45 m and 0.6 m × 0.6 m were measured for different controlled flow rates of the gas. The Froude (F) numbers, in the Cox and Chitty[1] experiments, range from 6×10^{-3} to 7.5×10^{-5}. The laboratory test results indicate that $p = 1$ for $10^{-4} < F < 10^{-3}$, $p = 2$ for $10^{-5} < F < 10^{-4}$ and $p = 0.4$–0.7 (Thomas' equation) for $F > 1.2 \times 10^{-3}$. Cox and Chitty provide the fire *L/D* data plotted against a modified Froude number (F_c), which is defined as the product of Froude number F and the Damkohler number, ·.

The above findings indicate that as the Froude number decreases (i.e., fire diameter become larger), the exponent value increases. Secondly, as the fire diameter gets larger than about 30 m the steady state liquid evaporation rate (due to heat feed back from the fire) decreases substantially, perhaps, due to significant radiant heat absorption in the unburnt bas bubble in the bottom part of the fire core. The combined effect of these two phenomena is to reduce the flame height to diameter ratio significantly for large fires compared to the predictions from currently used correlations. Therefore, it can be argued that for large LNG fires ($D > 30$ m) the correlations used in such models as LNGFIRE3 over predict the length of flame and, hence, the radiation hazard distance.

Fig. 6 shows the plot of fire plume length-to-diameter ratios from field LNG pool fire tests and the predictions from different correlations. Moorhouse [31] has not provided any physically or scientifically justifiable assumptions for his correlations; in addition, it is considerably different from other physics-based correlations and is, therefore, unacceptable. All field experiments to date involving LNG pool fires experiments have the Froude number values in the range $6 \times 10^{-3} < F < 3.5 \times 10^{-2}$ (or modified Froude number F_c, defined by Cox and Chitty, in the range $1 < F_c < 5.8$). Needless to say that the Cox and Chitty correlations with $p = 1$ or 2 are not applicable to conditions of the field LNG pool fire tests. This can be clearly seen in Fig. 1.

When F_c is greater than 1 the upward momentum of the released vapors (by liquid evaporation) is higher than that produced by buoyancy. Hence, the release momentum has a larger effect on the air entrainment and mixing. In a jet the value of FC is very high compared to 1, the *L/D* ratio becomes a constant independent of the F_c. In the case of buoyancy dominated fire ($F_c \ll 1$), the entrainment is dominated by buoyancy, and hence the *L/D* ratio is very dependent on the Froude number. In the region of interest for LNG fires in the open the momentum and buoyancy are some what in balance (with the former higher than the latter in smaller fires) and hence the exponent on the Froude number in the *L/D* correlation is between 0.4 and 0.7, the latter value more applicable to larger diameter fires.

Hightower et al. [25] postulate the occurrence of LNG fire diameters of 330 and 512 m due to releases from ships. For these diameters, the estimated Froude numbers (F) are, respectively, 1.98×10^{-3} and 1.59×10^{-3}. In these Froude number regions the Cox and Chitty correlation (with $p = 1$) is clearly not applicable. The values for the flame height-to-diameter ratios (*L/D*) used by Hightower et al. [25], based on Moorhouse correlation, for the above ranges of Froude numbers would therefore be,[2] 1.21 and 1.28, respectively. These are considerably higher than those predicted by Thomas' correlation (*L/D* = 0.87 and 0.75, respectively). All other things being equal the radiation hazard distances predicted by Hightower et al. are therefore, higher than what should be the case based on Thomas' correlation for flame heights, which is based on physical principles and experimental measurements.

3.1.2.1.3. Surface emissive power (E or SEP). Experimental values for the mean emissive power of LNG pool fires calculated on the basis of Thomas' correlation for the height of the visible (and, hence, assumed emitting surface) are presented in Table 1 and in Fig. 5. In using the emissive power values in models from these results the following issues need to be noted:

(1) The emissive power based on the actual fire surface area "seen" by an outside object is increasing as the diameter increases up to 35 m (see Fig. 5). However, the mean emissive power based on the idealized flame plume length (Thomas' correlation) seems to have decreased from the 15 m China Lake tests to the 35 m Montoir test. This is undoubtedly due to the effect of smoke obscuration in the latter tests.
(2) Recent assessment of the 35 m Montoir test spectral data indicates that the visible part of the fire is radiating at equivalent blackbody temperature of 1516–1525 K (corresponding emissive power 300–310 kW/m^2) and this fire is more or less optically thick (Malvos and Raj [14]). On the basis of analysis of fire spectral data the optical path length for a LNG pool fire is postulated to be 13.81 m (i.e., the extinction coeffi-

[1] Cox and Chitty define a modified Froude number (F_c), which is the product of the Froude number (F) defined in Eq. (6) and Damkohler number, $=\Delta H_c/(C_a T_a)$, where ΔH_c is the heat of combustion of the fuel per unit mass, C_a and T_a are, respectively, the specific heat at constant pressure and temperature of the air. Froude number F_c larger than 1 represents a situation in which momentum of vapors generated by boiling is higher than that due to buoyancy. The Cox and Chitty experiments span the range $1.25 \times 10^{-2} < F_c < 1$.

[2] The Sandia [25] report does not state, explicitly, the values used for the fire *L/D* ratios.

cient $\kappa = 0.0725\,m^{-1}$). Therefore, the gray body equivalent emissive power of those parts of the LNG fire that are not obscured by smoke can be represented by the equation

$$E_{\text{visible burning regions}} = E_B[1 - e^{-\kappa D}] \quad (9)$$

where, extinction coefficient $k = 0.0725\,m^{-1}$ and $E_B = 325\,kW/m^2$ (corresponding to 1547 K)

3.1.2.1.4. Multi-zone models. The models to calculate the fire radiation hazard should also consider the different regions of combustion within the height of the visible flame. Current generation models do not take these into consideration. It has been recognized in the fire literature that as the fire diameter increases the burning region is no longer represented by a columnar, cylindrical plume but consists of distinct zones. McCaffrey [39] proposed a three-zone model for a turbulent diffusion fire. The first zone consists of a fuel rich core region. In the second zone the flame is still anchored to the base but pulsates in size both radially and axially due to the effects of large scale eddies in the entrained air. The third zone, termed "the intermittency region" is where peeled off blobs of fuel burn in irregular clumps. While no specific calculation procedures are available to determine the heights of each zone, it is known that the first zone generally extends to about 10% of the visible flame height, the second zone varying between 10% and 40% of the flame height. It is obvious that the "top" of the burning flame ("flame height") is not a unique position in space but changes with time. Heskestad's [37] data indicates a correlation for the length of the intermittent zone (L_I) with the combustion Froude number F_c (for $7.5 \times 10^{-4} < F < 2.5 \times 10^{-1}$) as follows:

$$\frac{L_I}{L_F} = 0.167 - \log_{10}(F_c^{1/4}) \quad (10)$$

In the intermittent fire region, the flame is not coherent and, therefore, cannot be considered as a continuous emitter of radiation over the entire length of the intermittency region. New generation of LNG fire models must consider the effect of this phenomenon. It is appropriate to consider different values for the surface emissive power for the three regions. McGrattan et al. [26] have used a variation of this theme based on assumptions of the percent of combustion energy released, where all of the energy released is assigned to the first zone (and from which an effective height of uniform emissive power fire is determined). The application of this approach to LNG fire radiation assessment is questionable. This is because: (i) the percent of energy released is not a characteristic that is known a priori as a function of the burning rate, fuel properties, fire size, etc., (ii) the McGrattan et al., model divides the fire into two zones. The dimensions of the lower and upper zones are not specified nor or they related to any of the characteristics of the fire, such as its size, burn rate, etc., and (iii) all energy emanating from the fire is assigned to the bottom zone and none to the upper zone. This description of a fire cannot lead to correct estimation of hazard distances, especially in the case of an LNG fire in a dike where the bottom part of the fire may be masked by the dike wall.

Considine [29] presents a two-zone model, which consists of a region of visible flame extending from the base up to a fraction of the overall flame height with only slight obscuration by smoke. A second region above this region is postulated in which the hot flame gases periodically "bloom." By assuming a sinusoidal visualization of the hot inner region of the fire in the second region, it is shown that the average emissive power of the smoke obscured region is 0.3 times that in the un-obscured regions. The problem with this model is that there are many parameters in the sinusoidal representation (including a constant frequency). Also the relationship of the height of the "bottom" region with other fire parameters is undefined. Similar splitting of a fire into multiple zones for calculating the emission from fires based on smoke obscuration has been discussed by Rew and Hulbert [40].

3.1.2.1.5. Consideration of effect of smoke production and shielding. Large diameter LNG fires produce significant amount of smoke as seen in the Montoir experiments. This is similar to those observed in the burning of other higher hydrocarbon liquids (propane, butane, heavier oils, etc.) Two physical phenomena contribute to the production of smoke, even in "clean burning" fuels, such as LNG. The first is the lack of enough oxygen in the core of large diameter fires to burn the carbon produced by the pyrolysis of fuel vapor. This not only produces soot (carbon particles) but also lowers the overall heat release – and hence the temperature – resulting in the promotion of additional smoke production. The second phenomenon may be due to the lowering of the effective concentration of fuel and vapor in the core from the recirculation of burnt gases by the toroidal vortex that is prevalent in all large fires. The effect of smoke is to form a shield on the outer layers of the fire thereby reducing the effective emission of radiant heat flux from the fire. This has the effect of reducing, significantly, the thermal radiation hazard distance around large LNG (or other) fires. In addition, the formation (and recirculation) of smoke could result in less efficient combustion of the fuel and result in the lowering of the effective flame temperature. However, the reduction in the radiant emission out of the fire tends to increase the temperature of the gases. Which one of the two effects dominates depends on the chemical properties of the fuel, chemistry of combustion, the physical dimensions and the hydrodynamics of gas flow within the fire. Needless to state that consideration of all these phenomena makes a model very complex and not amenable to simple solutions; attempts are being made, however, to model these in CFD codes simulating large turbulent diffusion fires, with mixed results to date.

Soot is carbon particles (with diameters in the 3–30 nm) in a fire that are being oxidized and are "glowing"; in fact, the visibility of a fire is caused by the emission of radiation in the visible spectrum by the burning soot. When the carbon produced by pyrolysis is either partially oxidized or is not oxidized at all because of lower local temperature, carbon particles agglomerate to form long chain molecules of carbon or "smoke." Soot formation studies are extensively reported in the literature (for a listing of the relevant literature see Raj [41]). However, there is very little work on the measurement of smoke production rates in large turbulent diffusion fires. Notarianni et al. [42] measured the smoke production in crude oil fires of diameters from 0.085

to 17.2 m and found that smoke yield (mass fraction of burnt fuel that is emitted as smoke) increases as the diameter of the fire increases. The data for the mass fraction smoke yield (Y in %) versus fire diameter (D in meters) presented by these researchers can be correlated for crude oil fires as,

$$Y = 9.412 + 2.758 \log_{10}(D) \tag{11}$$

It is anticipated that the constants in the equation will depend very critically on the fuel chemical composition and pyrolysis properties. Unfortunately, such data do not exist for LNG fires. Considine [29] has discussed one approach to determining the effect of smoke in reducing the radiation by assuming an effective emissivity of the fire (in the regions of smoke production) to be about 0.3. This would typically make the LNG fire surface emissive power in the smoke regions to be about 65 kW/m^2. Delichatsios and Orloff [43] are able to correlate measured radiation from *optically thin flames* with burner size and fuel flow rate by postulating the soot concentration to be proportional to a fuel residence time scale (which depends upon the intensity of turbulence) and the reciprocal of the chemical formation time scale. This method is not applicable to large fires, which are optically thick and radiate in the H_2O and CO_2 bands. McCaffrey and Harkleroad [44] have presented soot data from small-scale experiments for a number of hydrocarbon fires in the form of specific extinction area (SEA) for soot. Experimental SEA values are, 124 m^2/kg for propane fires and 1000 m^2/kg for crude oil fires. No direct data for the smoke yield, as a function of fire diameter exists for large fires of different fuels.

3.1.2.1.6. Modeling smoke effects on radiation. Raj [35] has developed a semi-empirical LNG fire model (applicable to windless conditions or conditions in which the effect of wind is small compared to the phenomena that occur in very large diameter fires), which takes into consideration the various phenomena observed in large LNG (and other hydrocarbon) fires. The phenomena considered include: (i) the bottom part of the fire being very radiative, (ii) the dependency of the height of the "bottom region" upon fire size and liquid burning rate, (iii) the intermittent view of the inner burning "hot" regions of the fire in the region above the first region, (iv) the decrease of the frequency of "sighting" of the burning regions with height, (v) the effects of shielding by the smoke, (vi) emission from the hot smoke, etc. This fire model incorporates the results of correlations similar to those of Notarianni et al. [42] and McCaffrey and Harkleroad [44]. The result is a model in which the effective emissive power of the fire varies continuously from the top of the "bottom region" to the mean visible height up to which combustion of gases continue (within the fire). Equations to determine the relative heights of each zone and the variation of surface emissive power with height are presented. The model has been calibrated with the 35 m diameter Montoir test data and predicts the measured mean emissive power values from other tests conducted to date. It is calculated that for very large fires the smoke obscuration averaged SEP over the height of the fire (calculated using Thomas' correlation) is about 50% of the SEP values for fires sizes used in field experiments to date.

The effective emissive power in the smoke obscured regions is represented by,

$$E_{\text{eff}} = E_0 \tau_s \tag{12}$$

and

$$\tau_s = \text{transmissivity of smoke} = e^{-(k_m C_s L_b)} \tag{13}$$

Using the above model calculations have been made to "predict" the mean surface emissive power (SEP) of different size LNG pool fires, with the fire plume length being determined by Thomas' correlation (Eq. (6)). These results are presented in the paper by Raj [35]. It is seen that the model predicts reasonably well (within 15% for 15 m diameter and 2% for 35 m diameter fires) of the measured SEP's presented in Fig. 5 (or Table 1). Extrapolation to very large diameter fires (300 m diameter) indicates that the mean SEP will be about 60% of the values for the smaller diameter (15–35 m) fires. These calculated results are indicated in Table 3.

3.2. Vapor fire models

The procedure for calculating the thermal radiation hazard distances outside the fire spread zone of a deflagration vapor fire is similar to that used in pool fire hazard estimations, with one singular exception. The vapor fire is generally a fast moving fire and, therefore, the thermal heat flux at any one location changes with time both due to the changing distance from the fire as well as due to changing fire-to-object orientations. Daish et al. [22] have reviewed the available models in the literature. These models calculate the flame speed based on correlations similar to those shown in Fig. 8. The height of the "flash fire" is generally related to the width of burning (in the direction of fire travel) and the emissive power of the fire is close to 220–280 kW/m^2 as has been measured in the Coyote tests (Rodean et al. [22]).

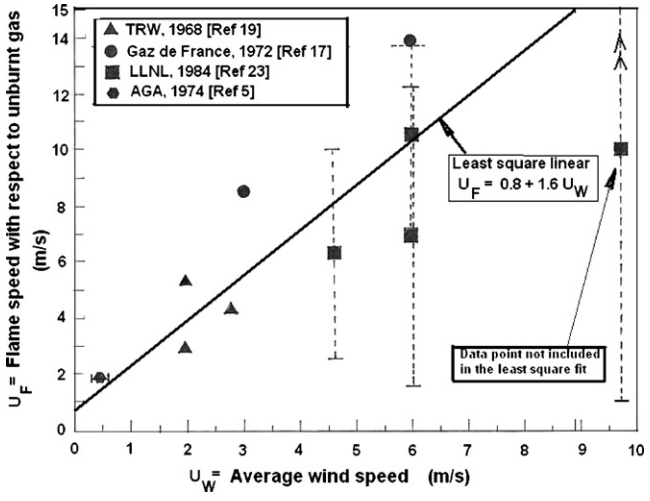

Fig. 8. Turbulent flame speed (relative to unburnt gas) in a LNG vapor cloud vs. average wind speed.

Table 3
Comparison experimental SEP data and predictions from the LNG pool fire model with smoke effects

Fire diameter (m)	Substrate on which LNG boils	Soot mass yield (Y)* (%)	Soot concentration (C_S) (kg/m^3)	Fractional length of the "Clean burning zone" (ψ)	Soot transmissivity (τ_s)	Mean SEP over the visible fire plume height[a] (E_{avg})		Remarks
						Current model result (kW/m^2)	From field tests (kW/m^2)	
15	Water	12.7	3.328×10^{-4}	0.255	6.64×10^{-1}	172	185–224	China Lake tests Raj et al. [7]
35	Land	13.7	3.595×10^{-4}	0.15	3.57×10^{-1}	177	175 ± 30	Montoir tests [13]
100	Land	14.9	3.926×10^{-4}	0.093	4.00×10^{-2}	113	–	Potential size of future pool fire tests
300	Water	16.2	4.272×10^{-4}	0.033	2.77×10^{-3}	90	–	Estimated pool size from one tank content spill from LNG ship

Source: Raj [35].
[a] Visible flame height determined using Thomas' equation: $L/D = 55[\dot{m}''/\rho_a\sqrt{gD}]^{2/3}[U_w/U_{ch}]^{-0.21}$; $U_{ch} = [(\dot{m}''/\rho_a)gD]^{1/3}$.

3.3. Atmospheric transmissivity

Raj [45] has calculated the absorption of thermal radiation from a black body at 1150 K for different path lengths through the atmosphere and different relative humidity values. The results are correlated by the dimensional equation:

$$\tau = 1.389 - \log_{10}\left[\left(\frac{\mathrm{RH}}{100}\right) p_w^{sat}(T_a) S\right] \quad (14)$$

$$P_w^{sat}(T_a) = \text{saturated water vapor pressure (N/m}^2\text{) at } T_a = e^{[25.81054-(5328.1/T_a)]}$$

Other correlations available in the literature for the atmospheric transmissivity of thermal radiation from a LNG fire are reviewed by Lees [46]. Several correlations are based on fire being assumed as a blackbody and account for absorption in the H_2O and CO_2 bands. Other correlations include the effect of scattering in the atmosphere. The following are some of these correlations from Lees [46].

$$\text{(i)TNO correlation : } \tau = 2.02\left[\frac{\mathrm{RH}}{100}\frac{p_w^{sat}(T_a)}{p_a} S\right]^{-0.09} \quad (15)$$

$$\text{(ii) major hazards assessment unit/HSE : } \tau = 1 - 0.058\ln(S) \quad (16)$$

$$\text{(iii) } \tau = 1.006 - 0.1171\log_{10}(X_{H_2O}) - 0.02368[\log_{10}(X_{H_2O})]^2 - 0.03188\log_{10}(X_{CO_2}) + 0.001164[\log_{10}(X_{CO_2})]^2 \quad (17)$$

where

$$X_{CO_2} = \left(\frac{273}{T_a}\right) S \quad (18)$$

and

$$X_{H_2O} = \left(\frac{288.651}{T_a}\right)\left(\frac{760}{101325}\right)\left[\frac{\mathrm{RH}}{100} p_w^{sat}(T_a)\right] S \quad (19)$$

Other parameters have the same definitions as indicated under Eq. (14).

4. Hazard prediction challenges

The above review of the literature indicates the complexity in evaluating properly the radiant heat emission from a LNG fire and assessing its hazard extent. The modeling difficulties arise in describing accurately: (i) the physical size of the fire for different circumstances of release (especially for unconfined LNG releases on water), (ii) the physical characteristics, such as the visible height, production of smoke, fraction of the fire area shielded by smoke, fire temperature in different regions, emissive power, etc. Added to this is the complexity of describing the damage that a particular level of thermal radiation (and

its intensity in various wavelengths) can cause in objects and human beings (a subject not discussed in this review). All current models are simplistic in their evaluation of the potential hazard zones, even though varying levels of complexity are considered in describing the emission from the fire and the absorption in the atmosphere. They all assume, in hazard distance calculations, an "open" field of view and do not take into account details of the effects of intervening objects (buildings, tress and other shelters) between the fire and the target object. Fire radiation, like ordinary light, is a line-of-sight phenomenon; any interruption of the "heat rays" results in shorter hazard distance. The consideration of such intervening objects is particularly important in establishing hazard zones in urban, industrial and residential areas.

The second important issue, not specified or considered in most of the models, is the characteristics of the receptor object. The thermal (and structural) response of an object exposed to radiant heat depends upon the intensity of radiant heat, the duration of exposure, radiative properties of the receptor surface (reflective, absorptive) and the thermal inertia of the body. In the case of human beings, the level of injury (damage) depends upon the percent of body (skin) exposed, the physiological reaction (sweating), effect of clothing protection, cooling by wind and above all the ability of the person to take shelter in a short period. In the US, the radiant heat flux criterion for evaluating people exposure hazard distance from LNG fires is 5 kW/m^2 for outdoor assembly of by groups of 50 or more persons and 9 kW/m^2 for exposure of buildings used for purposes of assembly, education, health care, residential or penal housing. No other criteria for hazards are specified (even though it is known that the extent of hazards/damages is dependent on the duration, area of exposure and the orientation of the body). The effects of any mitigating circumstances are not allowed to be considered. In the European Regulations, the people exposure hazard criterion is based on a modified total dosage unit (tdu) [tdu = $I^{4/3}t$, where I is the intensity of heat flux incident on the object and t is the duration of exposure]. The value of tdu to be used in hazard distance calculations depends upon the type of population being exposed (children, elderly, physically challenged, hospital patients, etc). For structural objects, the heat flux value is specified for the exposure criterion in both US and European regulations. Obviously, this will not suffice to determine the structural integrity of an object subject to radiant heat from a fire.

There are a number of shortcomings in most models that are used in facility siting assessments. These shortcomings are due to the omission of real phenomena in the models and the high degree of simplification (in the name of being conservative) to the extent that the hazard distance results are, perhaps, over estimated[3] by factors of 2 or 3. These results arise from the use of extremely conservative values for all parameters including: (i) the use of 300 kW/m^2 for the emissive power from the entire fire surface area in fires of diameters, which are at least one order of magnitude larger than the largest test fires, (ii) not considering properly the real phenomena, such as the production of smoke in large fires, atmospheric absorption of radiant heat, sensitivity of radiant heat absorption characteristics of the receptor to the spectral distribution of incident energy, effects of obstructions, etc.

5. Conclusions

The following conclusions are made from the review of the literature discussed in this paper:

(1) Large LNG pool fires burn with significant production of smoke, which masks the burning interior parts thereby reducing the overall radiant emission from the fire. The mean emissive power of large fires could be substantially smaller (by over a factor of 2) than observed in the 20 and 35 m diameter field fire tests.
(2) It is possible that very large LNG fires (of sizes 100 m and above in diameter) will look, both physically and radiatively, similar to other higher hydrocarbon (propane, butane, gasoline, etc.) fires with production of copious amount of black smoke and consequent reduction in radiative emission to out-of-fire environments.
(3) Large LNG spills on water in a relatively short period of time may result in substantial formation initially of high concentration vapor. If this vapor is ignited there exists a distinct possibility of generating a fireball type of burning. However, it is not certain whether this will constitute any greater hazard than if all of the spilled liquid spreads out and sustains a pool fire. This is because a significant part of the gas entrained in the fireball may not burn and secondly the lesser the amount of remaining LNG in the spreading pool the smaller will be the diameter of the pool fire (and hence the hazard distance).
(4) None of the vapor ignition tests in the open have produced anything other than a deflagration type flash fire burning to the source. Depending upon the location of ignition in the cloud some downwind movement of the fire has been seen. However, no flame acceleration (or the corresponding pressure increase in the vicinity) has been observed.
(5) It is uncertain whether a LNG vapor cloud, including a cloud containing higher concentrations of higher hydrocarbon vapors generated in the later stages of evaporation of a LNG pool, dispersed among obstructions, such as pipe racks, buildings, trees, houses, etc., and ignited by normal ignition sources will form an accelerating flame. Even if acceleration due to obstructions occurs, it is not certain that the magnitude of the acceleration will be sufficient to form a shock wave or even a wave of sufficient strength to increase

[3] Sandia report [25] lists, for an intentional breach scenario with release of 12,500 m^3 of LNG, the maximum pool size to be 405 m diameter, and the hazard distance to 5 kW/m^2 level to be 1579 m from the pool center. This calculation is based on the assumption of a fire height given by Moorehouse correlation; mean emissive power of the fire of 220 kW/m^2 and an atmospheric transmissivity of 0.8. If the more realistic values for a large LNG smoky fire are used [fire emissive power = 100 kW/m^2 (see Table 3), L/D ratio of 0.83 given by Thomas' equation] and with an atmospheric transmissivity of 0.5, the hazard distance reduces to 630 m, a reduction by a factor of 2.5!

the local pressure by appreciable amount (fractions of an atmospheric pressure). There are no field experimental data to make definitive statements.

(6) Thermal radiation hazard distance calculations must be balanced in the treatment of real physical effects. That is, not only should they consider the smokiness of large LNG fires but also: (i) consider the line of sight interruption effects by buildings, trees and other objects between the fire and the receptor, (ii) take into account the mitigation effects of clothing, physiological details of skin (reflectivity, absorptivity, cooling by sweat, etc) and (iii) include the realistic spectral description of the thermal radiation that reaches a person (after a part of the radiation, in H_2O and CO_2 bands, is almost completely absorbed by the intervening atmosphere).

(7) There is a need to revise the current criteria in the regulations for exposure to radiant heat for both structures and people. The revised criteria should: (i) take into account the duration of exposure or thermal dosage and (ii) consider specific spectral radiation absorption properties of the receptor surface as well as the physical, thermal and physiological properties of the receptor.

References

[1] http://www.dom.com/about/gas-transmission/covepoint/lng_history.jsp.

[2] P.K. Raj (Ed.), Volume III—Combustion and Radiation, Proceedings of MIT-GRI LNG Safety Workshop (March 22–24, 1982) held at MIT, Cambridge, MA 02139, published by the Gas Research Institute, Chicago, July 1982.

[3] H.G. May, W. McQueen, Radiation from large liquefied natural fires, Combust. Sci. Tech. 7 (1973) 51–66.

[4] D. Burgess, M.G. Zabetakis, Fire and Explosion Hazards of LNG, US Bureau of Mines Investigation Report # 6099, 1962.

[5] AGA, LNG Safety Program, Interim Report on Phase II Work, IS-3-1, American Gas Association, Arlington, VA, 1974.

[6] P.K. Raj, S. Atallah, Thermal radiation from LNG fires, Adv. Cryogenic Eng. 20 (1974) 143.

[7] P.K. Raj et al., Experiments Involving Pool and Vapor Fires from Spills of LNG on Water, NTIS # AD-A077073, USCG Report, Washington, DC 20590, 1979.

[8] JGA, A study of dispersion of evaporated gas and ignition of LNG pool resulting from continuous spillage of LNG, J. Jpn. Gas Assoc., July 1976.

[9] D.J. Moorhouse, Scaling criteria derived from large scale experiments—the assessment of major hazards, Inst. Chem. Eng., Manchester (1982).

[10] G.A. Mizner, J.A. Eyre, Large scale LNG and LPG Pool Fires, Inst. Chem. Eng. Symp., Ser. 71, Manchester (April 1982).

[11] G.A. Mizner, J.A. Eyre, Radiation from liquefied gas fires on water, Combust. Sci. Technol. 35 (1983) 33–57.

[12] H. Kataoka, Report on LNG Anti-disaster Experimental Test, Report by Tokyo Gas Co., Ltd., Japan, 1981.

[13] D.J. Nedelka, J. Moorhouse, R.F. Tucker, The Montoir 35 m Diameter LNG Pool Fire Experiments, TRCP.3148R, 9th Intl. Conf. & Expo on LNG, LNG9, Nice, France, 1989.

[14] H. Malvos, P.K. Raj, Details of 35 m Diameter LNG Fire Tests Conducted in Montoir, France in 1987 and Analysis of Fire Spectral and other Data, paper presented at the 2006 Spring National Meeting of the AIChE, Session VI, LNG Safety, Orlando, FL, April 2006.

[15] P.K. Raj, LNG Fire Spectral Data and Calculation of Emissive Power, Paper presented at the International Symposium on Process Safety, Mary Kay O'Connor Process Safety Center, Texas A&M University, October 25 and 26, 2005, College Station, TX, Paper accepted for publication in the Journal of Hazardous Materials, 2006.

[16] H.C. Gollahalli, H.F. Sullivan, Effect of Pool Shape on Burning Rate, Radiation and Flame Height of liquid Pool Fires, Report by the Department of Mechanical Engineering, University of Waterloo, Ontario, Canada, 1974.

[17] P.A. Croce, K.S. Mudan, J. Moorhouse, Thermal Radiation from LNG Trench Fires—Volume I, Report # GRI 84/0151.1, Gas Research Institute, Chicago, IL, September 1984.

[18] Gaz de France, Essais D'Ependage de Gaz Naturel Liquefie Sur de Sol, Report on the experiments conducted by Gaz de France, September 1972.

[19] TRW, An Experimental Investigation of Atmospheric Diffusion and Ignition of Boil-Off Associated with a Spillage of Liquefied Natural Gas, TRW, Inc., Film section of the Report # 08072-7 for the AGA, November 1968.

[20] AGA, LNG Safety Program, Interim Report on Phase II work, American Gas Association, Project IS-3-1, July 1974.

[21] P.K. Raj, H.W. Emmons, On the Burning of a Large Flammable Vapor Cloud, paper presented at the meeting of the Western & Central States Section of the Combustion Institute, San Antonio, TX, April 1975.

[22] H.C. Rodean, W.J. Hogan, P.A. Urtiew, H.C., Goldwire Jr., T.G. McRae, D.L. Morgan Jr., Vapor burn analysis for the Coyote series LNG spill experiments, Lawrence Livermore National Laboratory, Rep # UCRL-53530, 1984.

[23] N.C. Daish, P.F. Linden, V. Vieillard, D. Nedelka, T.A. Roberts, C.J. Butler, A new unified investigation into vapour cloud fires, in: Proceedings of LNG13, 13th International Conference and Exhibition on Liquefied Natural Gas, Seoul, Korea, 2001.

[24] T.C. Brown et al., 1987 LNG Vapor Barrier Verification Field Trials—Falcon Series Data, Final report, Gas Research Institute, GRI-89/0138, 1990.

[25] M. Hightower, L. Gritzo, A. Luketa-Hanlin, J. Covan, S.Tieszen, G. Wellman, M. Irwin, M. Kaneshige, B. Melof, C.Morrow, D. Ragland, Guidance on Risk Analysis and Safety Implications of a Large Liquefied Natural Gas (LNG) Spill Over Water, Sandia National Laboratory Rep.# SAND2004-6258, U.S. Department of Energy, Washington, DC, December 2004.

[26] K.B. McGrattan, H.R. Baum, A. Hamins, Thermal Radiation from Large Pool Fires NISTIR 6546, National Institute of Standards & Technology, U.S. Department of Commerce, Washington, DC, November 2000.

[27] H.C. Hottel, A.F. Sarofim, Radiative Transfer, McGraw-Hill Book Company, New York, 1967.

[28] D.J. Moorhouse, M.J. Pritchard, Thermal radiation hazards from large pool fires and fireballs—a literature review, Inst. Chem. Eng. Symp. (71) (1982) 397–428.

[29] M. Considine, Thermal Radiation Hazard Ranges from Large Hydrocarbon Pool Fires, Report # SRD R297, Safety & Reliability Directorate, UK Atomic Energy Authority, Wigshaw Lane, Culcheth, Warrington, WA3 4NE, UK, October 1984.

[30] SFPE, The SFPE Handbook of Fire Protection Engineering (second ed.), 1995 (ISBN 0-87765-354-2 (NFPA No. HFPE-95)).

[31] D.J. Moorhouse, Scaling criteria derived from large scale experiments—the assessment of major hazards, Inst. Chem. Eng. Symp. (71) (1982) 165–179, Manchester.

[32] LNGFIRE III, A Thermal Radiation Model for LNG fires, GTI-04/0032, Gas Technology Institute, Chicago, March 2004.

[33] P.H. Thomas, Fire spread in wooden cribs: Part III, The effect of wind, Fire Research Note No. 600, Fire Research Station, Boreham Woods, England, June 1965.

[34] P.H. Thomas, The Size of Flames from Natural Fires, in: Ninth Symp (int'l) Combustion, Academic Press, New York, 1963, pp. 844–859.

[35] P.K. Raj, Large Hydrocarbon Fuel Pool Fires, Physical Characteristics and Thermal Emission Variations with Height, Paper accepted for publication in JHM, Aug 2006, Appendix A of the paper describes Relationship between visible fire plume height, diameter and burning rate.

[36] M.P. Murgai, Natural Convection from Combustion Sources, Oxford & IBH Publishing, New Delhi, 1976.

[37] G. Heskestad, Luminous heights of turbulent diffusion flames, Fire Saf. J. 5 (1983) 103–108.

[38] G. Cox, R. Chitty, Some source-dependent effects of unbounded fires, Combust. Flame 60 (1985) 219–232.

[39] B.J. McCaffrey, Momentum implications for buoyant diffusion flames, Combust. Flame 52 (1983) 149–167.

[40] P.J. Rew, W.G. Hulbert, Development of Pool Fire Thermal Radiation Model, HSE Contract Research Report No. 96-1996, Health and Safety Executive, 1996.
[41] P.K. Raj, Large LNG fire thermal radiation—modeling issues and hazard criteria revisited, (AIChE) Process Saf. Prog. 24 (September (3)) (2005).
[42] K.A. Notarianni, D.D. Evans, W.D. Walton, D. Madrzykowski, J.R. Lawson, Smoke production from large oil pool fires, in: C.A. Franks (Ed.), Interflam '93, Fire Safety, Int'l Fire Conference, 6th, Oxford, England, Interscience Communications Ltd., London, England, March 1993, pp. 111–119.
[43] M.A. Delichatsios, L. Orloff, Effects of turbulence on flame radiation from diffusion flames, in: Twenty-Second Symp. (Int'l) on Combustion, The Combustion Institute, 1988, pp. 1271–1279.
[44] B.J. McCaffrey, M. Harkleroad, Combustion efficiency, radiation, CO and soot yield from a variety of gaseous, liquid and solid fueled buoyant diffusion flames, in: Twenty-Second Symp. (Int'l) on Combustion, The Combustion Institute, 1988, pp. 1251–1261.
[45] P.K. Raj, Calculations of Thermal Radiation Hazards from LNG fires—A Review of the State-of-the-Art, paper # 2, Session 18, AGA Transmission Conference, St. Louis, MO, May 1977.
[46] F.P. Lees (Ed.), Loss Prevention in Process Industries, Hazard Identification, Assessment and Control, second ed., Butterworth-Heinemann Linacre House, Jordan Hill, Oxford, 1996, section 16.13.9, OX2 8DP.

Glossary

AGA: American Gas Association
LNG: Liquefied natural gas
LFL: Lower flammable limit
RPT: Rapid phase transition
SEP: Surface emissive power. Also used for spot emissive power
tdu: Total dose unit [in units $(kW/m^2)^{4/3}$ s]
UFL: Upper flammable limit